Materials Research. 2021; 24(4): e20200508
DOI: https://doi.org/10.1590/1980-5373-MR-2020-0508

Preparation and Application in Crude Oil-Water Separation of Clay-Based Membranes

Mykaell Yan Muniz de Souza[a]*, *Hélio de Lucena Lira*[a], *Lisiane Navarro de Lima Santana*[a], *Miguel Angel Rodríguez*[b]

[a]*Universidade Federal de Campina Grande (UFCG), Departamento de Engenharia de Materiais, Av. Aprígio Veloso, n° 882, Bodocongó, Campina Grande, PB, Brasil*
[b]*Instituto de Cerámica y Vidrio, CSIC, C/Kelsen, 5, 28049 Madrid, Spain*

Received: November 09, 2020; Revised: March 30, 2021; Accepted: May 11, 2021

In this study, tubular ceramic membranes were prepared from a mixture of ball clay, talc and alumina. The mixture was characterized by the following techniques: particle size analysis, X-ray fluorescence spectroscopy (XRF), X-ray diffraction (XRD) and thermal analysis. Tubular membranes were produced by extrusion process and thermal treated at temperatures between 1025 °C and 1175 °C. The membranes were characterized by XRD, linear shrinkage, apparent porosity, flexural strength, mercury porosimetry, scanning electron microscope (SEM) and contact angle. To evaluate the efficiency of the membranes, permeability tests with distilled water and oil-in-water emulsion were conducted in a tangential flow system. The results showed that the sintering of the specimens promoted the formation of α-cordierite phase and directly influenced the physical and mechanical properties such as linear shrinkage, porosity and flexural strength. Separation tests revealed that these membranes promoted high oil-water separation efficiency with values above 99.0%.

Keywords: *Clays, sintering, cordierite, membranes, microfiltration, oily wastewater.*

1. Introduction

Ceramic membrane technology has been presented as a promising method of separation in environmental applications such as pretreatment of industrial effluents and wastewater treatments[1-3]. During the last years, ceramic membranes have been attracted the attention of the industries and researchers centers due their desirable properties such as chemical durability, high mechanical and thermal stability and high separation efficiency[4-6].

Lots of commonly available materials such as alumina, titania, zirconia and silica and their combinations are widely used for preparation of ceramic membranes. These inorganic precursors are very expensive and require high sintering temperature for fabrication[7]. For this reason, it is important to develop low cost materials and fabrication techniques for ceramic membranes.

In this way, many researchers have been focused to prepare low-cost ceramic membranes using natural raw materials due their abundance all over the world and to use of lower sintering temperatures than those needed for metal oxide-based materials[8-14].

In particular, the Brazilian northeast has many deposits of clays that show great potential in several applications for ceramic industry, especially in ceramic membrane manufacturing[15-18]. Therefore, the sintering of clay-based compositions leads to the formation of important crystalline phases that have great influence on physical and mechanical properties of ceramic pieces. One of the most important is cordierite, which is usually obtained from firing of mixture containing clays, talc and alumina and/or magnesia[19].

Tubular ceramic membranes are especially suitable in applications where the feed stream contains a relatively high proportion of large particles and where the membranes are exposed to extreme pH and temperature conditions[20]. Therefore, tubular ceramic membranes allows to obtain higher flux and more efficient separation[21,22].

Oily wastewater is generated in many process industries such as petrochemical plants, refinery, metallurgy, and transportation. Due the high volume and complexity, this effluent should be treated and reduced to an acceptable limit before discharged into the aquatic environment[23-27]. According to Brazilian standards, the maximum concentration of oil and grease in water before released into seas must be 29 (mg/L)[28]. On the other hand, according to some researchers, the allowable limit of oil and grease concentration in industrial effluent based on international standards must be (10 – 15 mg/L)[2,29,30].

Currently, the development of low cost ceramic membranes from natural raw materials for oily wastewater treatment are discussed by some researchers. Kumar et al.[31] elaborated tubular ceramic membranes using a mixture of ball clay, feldspar, kaolin, pyrophyllite and quartz. The membranes (porosity of 50.0% and average pore diameter of ~0.34 μm) were tested on the separation process of oil-in-water emulsion with a feed concentration of 100 mg/L and exhibited oil rejection of 99.9%. Abbasi et al.[30] synthesized mullite tubular membranes using a kaolin clay-based composition. They investigated the performance of the prepared membranes for treatment of oily wastewater at different oil feed concentrations

*e-mail: mykaell.yan@gmail.com

(250 – 3000 mg/L) and obtained 94.5% of oil rejection. Nandi et al.[2] developed low cost ceramic membranes using natural raw materials as kaolin, quartz, and feldspar and showed satisfactory results of permeability at different oil feed concentrations (125 – 250 mg/L) with great results of oil rejection (98.8%).

In this context and to contribute to both scientific and technology aspects, the aim of this work is to prepare and applied in crude oil-water separation clay-based membranes from a mixture of ball clay, alumina and talc. The selection of these raw materials was based on their low cost and abundance in the Brazilian northeast region.

2. Experimental

In this work, ball clay and talc were supplied by a mineral company located in the Paraíba state, Brazil, and alumina was provided from Treibacher Schleifmittel Brazil Ltda. Crude oil collected from Piranema oil-field exploration located in the state of Alagoas, Brazil was used for preparation of oil-water emulsion. Crude oil samples were collected at 1200 m of depth and have API grade 41-43.

The formulation was defined from the chemical analysis of raw materials and based on stoichiometric composition of cordierite ($2MgO.2Al_2O_3.5SiO_2$) in the SiO_2-Al_2O_3-MgO ternary system. It was established the following percentages: 23 wt.% of ball clay, 19 wt.% of alumina and 58 wt.% of talc. The chemical composition of raw materials and the formulation are described in Table 1.

The formulation was previously passed in a sieve ABNT n° 200 (0.075 mm) and submitted to the following techniques: chemical analysis using energy dispersive X-Ray Fluorescence spectroscopy (XRF) (Shimadzu, EDX 720); particle size analysis (Cilas, 1064 LD); thermogravimetric (TGA) and differential thermal analysis (DTA) at a heating rate of 10°C/min up 1200 °C under atmospheric air (Shimadzu, DTG-60H); and mineralogical composition using X-ray diffraction (XRD) (Shimadzu XRD 6000 diffractometer) with Cu Kα radiation (40 Kv/30 mA), using a goniometer rotation of 2°/min and a step scan of 0.02°, in the range from 5° to 60°. It was also estimated the plasticity index of the mixture measuring the Atterberg limits.

The homogenization of the mixture was held in a mixer at 130 rpm for 24 hours with distilled water to formation desired plastic paste. The specimens were shaped into a tubular configuration using a vacuum extruder (Sew Brazil Ltd., model 3FAS). The pieces were oven-dried at 110° C for 24 hours and sintered in furnace (MAITEC, FSQC 1300/3) at temperatures of 1025, 1050, 1075, 1100, 1125, 1150 and 1175°C, at a heating rate of 5°C/min and dwell time of 60 min in each maximum temperature. Figure 1 shows tubular pieces before and after sintered at different temperatures.

After the heat treatment, the ceramic pieces were submitted to mineralogical characterization by XRD following the same conditions previously mentioned. The phases formed at each temperature were identified using JCPDS standards cards available in a PCDF WIN software program database of the Shimadzu XRD 6000 diffractometer.

The ceramic pieces were characterized by the following physical properties: linear shrinkage and apparent porosity (Archimedes' Principle). The flexural strength of sintered samples was measured using Shimadzu equipment (Autograph AGX-50 KN) with a maximum lead of 50 KN and a loading speed of 0.5 mm/min.

The average porous size distribution was estimated using a mercury porosimetry (AutoPore IV 9500 V1.09). The fracture surface of the sintered samples was analyzed by scanning electron microscope (SEM) (Shimadzu 5SX MCB-550). The contact angle of the membranes was determined using a contact angle portable equipment (Surface Eletro Optics – SEO, Phoenix-I model).

Oil-in-water emulsion was prepared from crude oil to investigate the efficiency of membrane separation. A stable and homogeneous oil-in-water emulsion with a concentration of 200 mg/L was prepared by mixing crude oil, surfactant agent and distilled water and using a Turrax mixer at a speed of 17000 rpm for 30 min.

The permeability of the membranes (10 mm of outer diameter, 7 mm of inner diameter and 77 mm in length) was evaluated using a tangential flow laboratory system (Figure 2). The membrane permeation was determined using distilled water and oil-in-water emulsion with concentration of 200 mg/L. The tests with distilled water were performed at different pressures of 1, 2 and 3 bar. To the treatment of

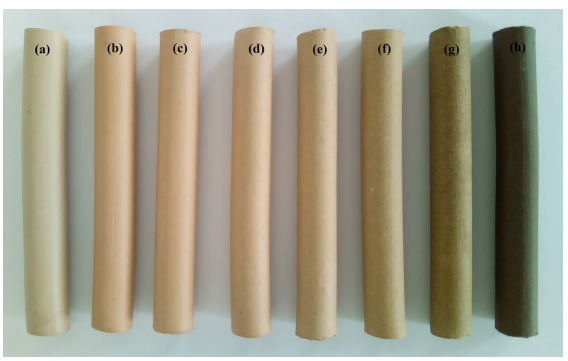

Figure 1. Tubular pieces (a) dried at 110 °C and sintered at different temperatures: (b) 1025 °C, (c) 1050 °C, (d) 1075 °C, (e) 1100 °C, (f) 1125 °C, (g) 1150 °C and (h) 1175 °C.

Table 1. Chemical composition (wt.%) of the raw materials and formulation.

Component	Oxides							
	SiO_2	Al_2O_3	MgO	Fe_2O_3	CaO	K_2O	TiO_2	Other oxides
Ball Clay	57.9	30.0	1.9	3.3	4.7	0.5	0.6	1.1
Alumina	0.3	99.2	-	-	0.2	-	-	0.3
Talc	55.1	12.3	20.5	7.8	2.6	0.5	0.2	1.0
Formulation	43.3	32.5	12.5	7.3	3.0	0.5	0.3	0.6

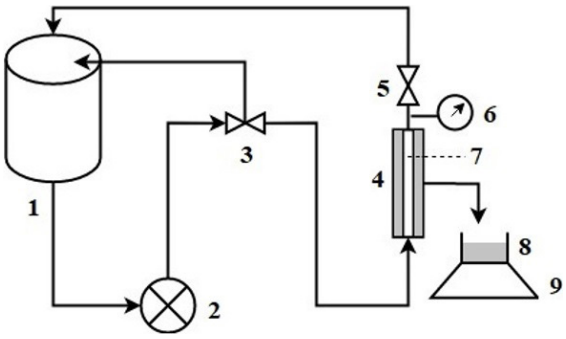

Figure 2. Schematic diagram of the tangential flow laboratory system. 1: Feed tank, 2: pump, 3: by-pass valve, 4: membrane module, 5: pressure gauge, 6: manometer, 7: membrane, 8: permeate and 9: electronic balance.

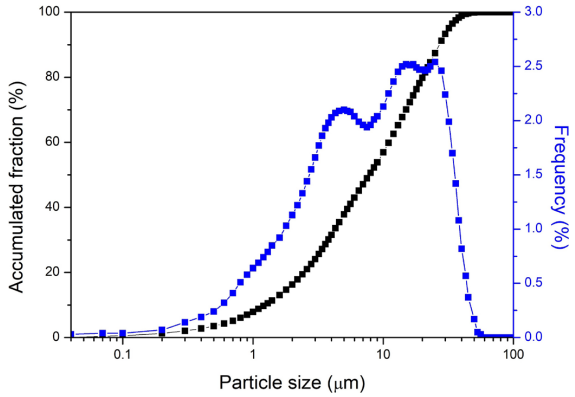

Figure 3. Particle size distribution curves of the formulation.

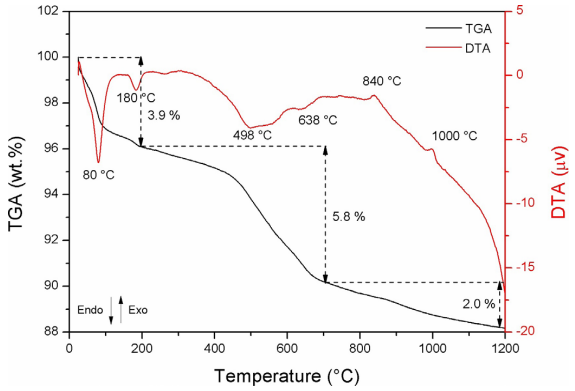

Figure 4. DTA and TGA curves of the formulation.

oil-in-water emulsion it was used a pressure of 3 bar (the best operating conditions). The permeate was collected at intervals of 3 min to verify the variation of flux for a period of 60 min of operation. All these experiments were conducted using four membranes for each temperature. The effective membrane surface area in contact with the feed was equal to $1.42x10^{-3}$ m^2. To evaluate the efficiency of the membranes, the feed solution and permeate samples collected after filtration were subjected to the turbidity technique. The oil present in the permeate samples was measured by using a microprocessed digital turbidimeter (Dellab).

3. Results and Discussion

The chemical composition of the raw materials and formulation before firing are shown in Table 1.

The most abundant oxides present in the formulation are SiO_2, Al_2O_3 and MgO. These contents were close to stoichiometric composition of cordierite (51.4% of SiO_2, 34.9% of Al_2O_3 and 13.7% of MgO). There is also a relevant content of Fe_2O_3 and CaO and a small amount of K_2O. These oxides can promote the formation of liquid phase at low temperatures and favoring the reduction of sintering temperature[32-34]. In particular, the presence of transition metal oxides as Fe_2O_3 and TiO_2 can promote the crystallization of cordierite phase in the ternary system SiO_2-Al_2O_3-MgO[35,36].

Figure 3 illustrates the particle size distribution curves of the mixture used to make the ceramic membranes. The granulometric distribution of the mixture shows a bimodal behavior with a wide distribution in the range of 1 - 50 μm, a mean particle diameter of 11.0 μm and accumulated volumes of D_{10} = 1.2 μm, D_{50} = 7.8 μm and D_{90} = 26.1 μm. The curves show a considerable number of particles with size below 20 μm, which are associated to the presence of finer particles from the clay. The particle size distribution is an important factor due its influence on the processing characteristics as plasticity, packing and the kinetic of the reactions to formation of important crystalline phases[37]. The plasticity index is 28% and is accordance to the values indicated in literature for ceramics paste be processed by extrusion, since the mixture shows a highly plasticity greater than 15%[38].

The curves of the thermal analysis are illustrated in Figure 4. The DTA curve shown endothermic peaks at 80 and 180 °C, corresponding to the removal of weakly bound water; between 450 and 650 °C appear endothermic effects that are associated with the structural collapse of the clay minerals; an exothermic peak is observed at 840 °C, related to the formation of enstatite from decomposition of talc; and another exothermic peak is observed at 1000 °C, attributed to the nucleation of crystalline phases as spinel[39] or sapphirine[40]. According to the TGA curve, three stages of mass loss are observed, the first stage takes place between 25 and 200 °C with mass loss of 3.9%, which represents loss of absorbed water; the second stage, between 200 and 700 °C, with strong mass loss of 5.8%, corresponding to dihydroxylation of clay minerals; the third stage, above 700 °C, with mass loss of 2.0% is associated to the carbonates decomposition, as well as the elimination of hydroxyl groups from talc[41]. In total, the formulation showed a mass loss of 11.7%.

The XRD patterns of the samples before and after firing at 1025 and 1175 °C are represented in Figure 5. Before heat treatment, it was identified the following crystalline phases: montmorillonite (JCPDS 13-0135), kaolinite (JCPDS 29-1490) and talc (JCPDS 83-1768). It was also observed the presence of accessory minerals such as quartz (JCPDS 46-1045), calcite (JCPDS 89-1305) and α-alumina (corundum) (JCPDS 10-0173).

At 1025 °C, the mineralogical phases observed are: cristobalite (JCPDS 82-0512), enstatite (JCPDS 86-0430), hematite (JCPDS 89-8104), α-alumina, quartz (JCPDS 46-1045) and sapphirine (86-2245 JCPDS). The presence of enstatite

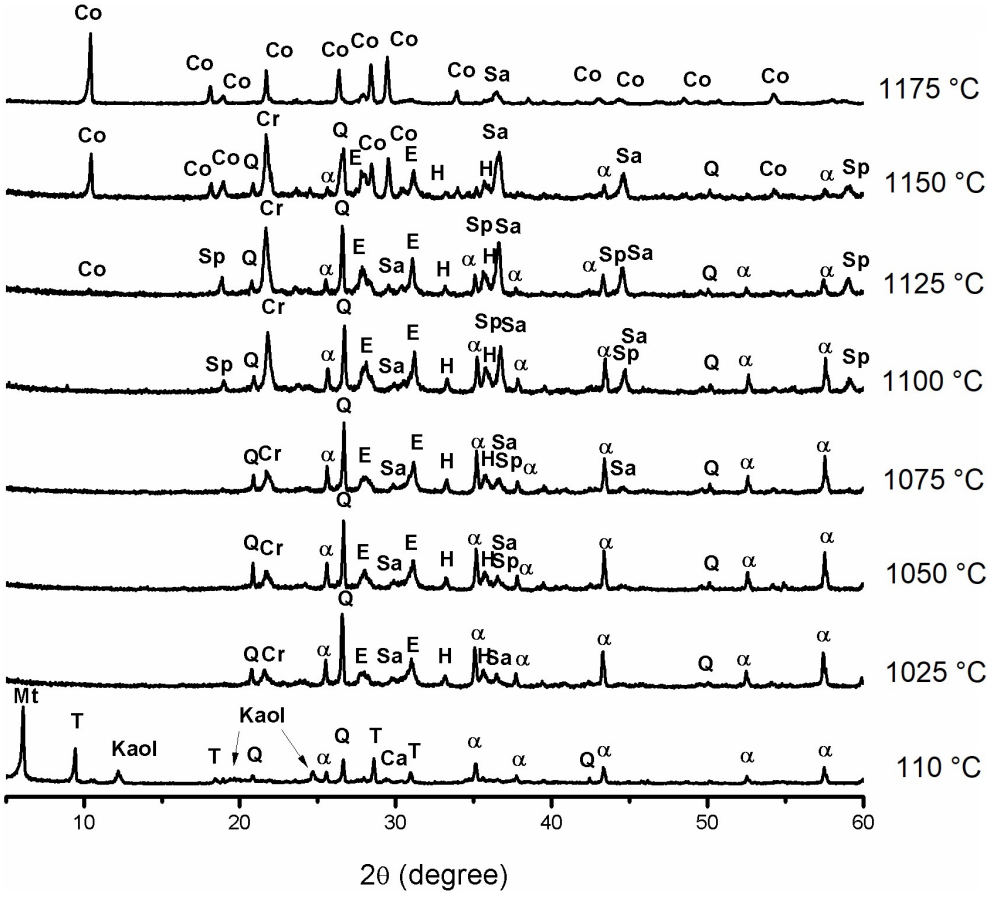

Figure 5. X-ray diffraction patterns of the sintered samples. α: Corundum, Co: α – cordierite, Cr: Cristobalite, Ca: Calcite, E: Enstatite, H: Hematite, Kaol: Kaolinite, Mt: Montmorillonite, Q: Quartz, Sp: Spinel, Sa: Sapphirine, T: Talc.

is related with the decomposition of talc, corroborating with the results from thermal analysis. Some authors observed this reaction between 800 – 1000 °C[33,42,43]. The formation of cristobalite is due to crystallization of amorphous silica from the clay mineral breakdown during the thermal reactions[44]. The sapphirine (JCPDS 21-0549) results from the reaction of cristobalite and intermediate phases[45]. The hematite phase is due to the iron oxide present in the formulation.

At 1050 °C, the formation of spinel phase was observed (JCPDS 77-0435) and according to Majumder et al.[46], this phase is a result of the interaction between Al^{3+} and Mg^{3+} ions dispersed in liquid phase. From 1075 °C to 1100 °C, the peaks intensity of cristobalite, enstatite and sapphirine increased, suggesting higher degree of crystallinity.

At 1125 °C, peaks intensity of spinel, alumina and hematite decreased and α-cordierite (indialite) (JCPDS 83-2067) was detected. According to Al-Harbi et al.[47], the crystallization of this phase is mainly due to the direct reaction between spinel and amorphous silica. These authors also identified the nucleation of α-cordierite phase at 1125 °C from the sintering of kaolinite and magnesite.

From 1125 to 1150 °C, the peak intensity of α-cordierite increases and peaks intensity of hematite decreases, indicating a possible thermal decomposition of hematite phase or probably the iron ions migrating to the structure of α-cordierite, forming a solid solution[35]. The α-cordierite (α-$Mg_2Al_4Si_5O_{18}$) structure is not fixed, because total or partial substitution occur between Mg^{2+} ions and Fe^{2+} ions, resulting in a similar structure ($Fe_2Al_4Si_5O_{18}$) known as iron cordierite[48]. According to studies by others researchers[19], the iron can be present as substitutional ions in cordierite structure but also as oxide impurities.

At 1175 °C, α-cordierite becomes the main crystalline phase accompanied by sapphirine, while the other secondary phases such as alumina, cristobalite, enstatite, hematite and spinel were not detected, probably indicating total dissolution. The formation of α-cordierite is a result from the decomposition and reaction between these secondary phases and was detected at temperatures close to 1200 °C[47,49-54].

The results of linear shrinkage and apparent porosity of the sintered samples are presented in Figure 6. It is noted that the sintering temperature has an influence on these properties. The linear shrinkage of all specimens increased with values ranged from 2.5 ± 0.2 to 6.0 ± 0.2% when the temperature increased from 1025 to 1175 °C, respectively. An accentuated change in linear shrinkage is observed when the temperature is above 1075 °C, which indicate a beginning of the densification process, induced by the formation of the liquid phase due to the presence of the alkaline and alkaline-earth oxide content in the starting raw materials[6]. In fact, according to the chemical analysis, the starting raw materials showed a considerable amount of fluxes oxides (Fe_2O_3 and

CaO) which can promote the formation of liquid and glassy phases. Regarding apparent porosity, the highest value was found in the sample sintered at 1025°C presenting an average of 36.5 ± 0.2%. As can be seen in the Figure 6, there was no significant variation between the samples sintered at 1025 and 1075° C, but a sharply decrease at 1075 °C and which continues during the firing process up to 1175 °C, reaching a value of 2.9 ± 0.6%.This is explained by the fact that the increasing in sintering temperature accompanied by the formation of liquid phase and densification process, lead a fill of pores causing the reduction in porosity[6].

The ceramics membranes should present high porosity and the tubes sintered at 1025, 1050, 1075 and 1100 °C showed satisfactory porosities and were considered for further study.

Figure 7 shows flexural strength as a function of sintering temperature. The increase in the sintering temperature tends to enhance the mechanical behavior of the ceramic pieces. The mechanical strength values ranged from 25.3 ± 3.3 to 71.5 ± 6.5 MPa when the temperature increases from 1025 to 1175 °C, respectively. This increase on the mechanical properties is explained by the decrease in porosity of the samples due the formation of liquid phase and glassy phase during firing process. In fact, a correlation between the results of porosity and flexural strength shows that the highest modulus of flexural strength is observed at 1175 °C, when the samples reached the lowest value of porosity. Another fact that may have contributed to the increase in mechanical resistance is associated to the intensification of crystalline phases. As showed by the XRD patterns, with increasing temperature from 1150 to 1175 °C, the peaks of α-cordierite phase become more intense and this contribute to increase the modulus of flexural strength. According to some researchers[54,55] the growth of cordierite crystals and densification process during sintering process have great influence on the mechanical behavior of the cordierite ceramics. The values of flexural strength of the samples were quite similar to those reported by other researchers[8,20,56,57].

The pore size distribution for the tubes sintered at different temperatures is represented in Figure 8. The pore size distributions of the samples are uniform (mono-modal distribution) and homogeneous. The majority of pores have diameters smaller than 2 μm, ranging from 0.2 to 2 μm for all samples. The average pore size diameters are 0.6, 0.8, 0.9 and 0.9 μm for the samples sintered at 1025, 1050, 1075 and 1100 °C, respectively. A slightly increase in the average pore size diameters is observed with the sintering process. As expected, the increasing temperature promotes the formation of liquid phase during the sintering process, which by capillarity effect fill the small pores leading to the reduction of porosity or even the disappearance of these pores and promoting coalescence of larger pores[16,58]. This phenomenon is clearly observed from the curves distributions, since these curves tend to move to the right side with increasing temperature[58]. The pore size is an important factor that define the application for ceramic membranes. Especially for the application in microfiltration process is expected that the ceramic membranes show pores sizes between 0.1 and 10 μm[6,59]. All the prepared membranes present porous diameters close to 1.0 μm with satisfactory porosity. In this way, these tubes should be considered for further study and used in microfiltration process.

SEM images of cross section of the tubes fired at 1025, 1050, 1075 and 1100 °C are shown in Figure 9. The morphology of each tube present pores with different formats over the cross section. There is no significant difference between the

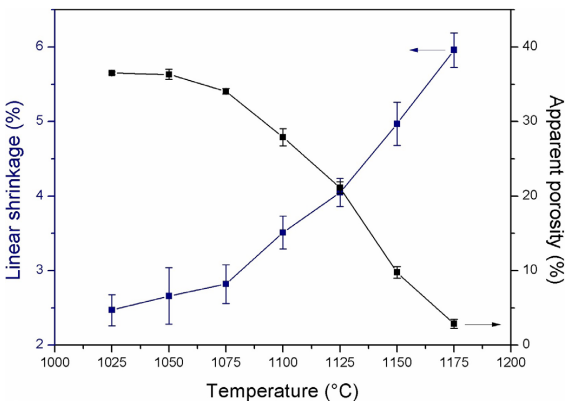

Figure 6. Linear shrinkage and apparent porosity of the sintered samples.

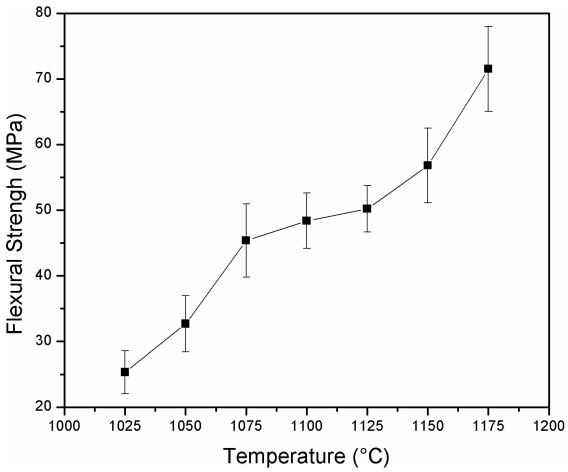

Figure 7. Flexural strength of the tubes.

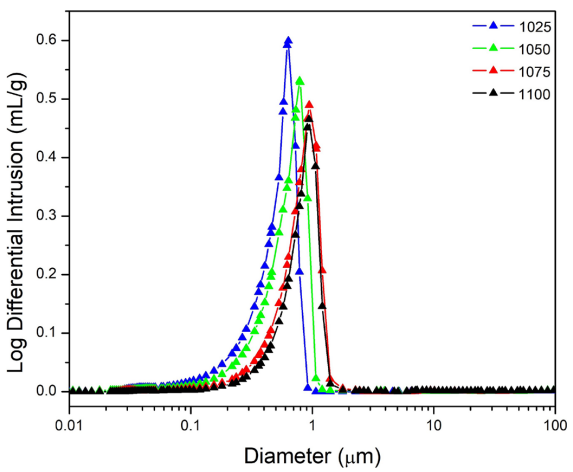

Figure 8. Porous size distribution curves of the prepared membranes.

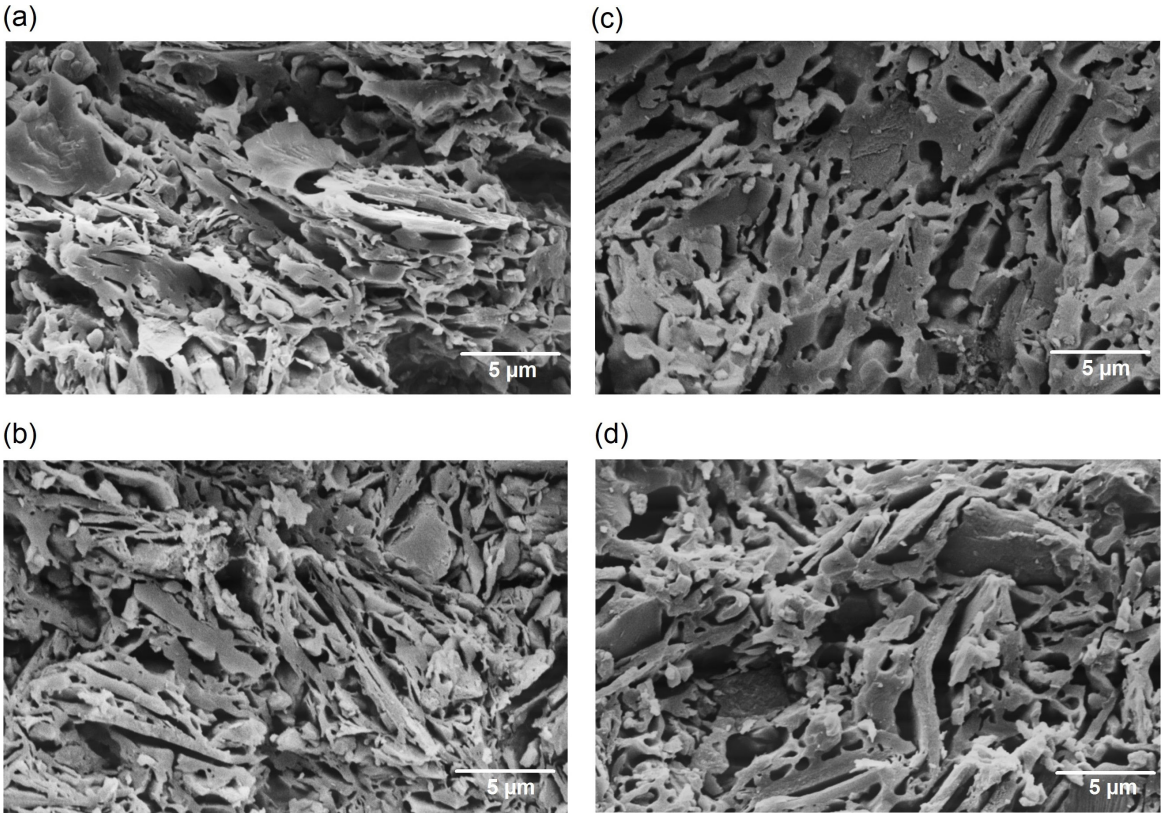

Figure 9. SEM images of inner surfaces and cross section of the tubes sintered at (a) 1025 °C, (b) 1050 °C, (c) 1075 °C and (d) 1100 °C.

samples, indicating that the pores have not changed gradually with the sintering process.

Figure 10 exhibit the images obtained from the contact angle analysis performed with the membranes. From this technique, the following values were obtained: 14.5, 13.1, 14.8 and 12.3, observed in membranes sintered at 1025, 1050, 1075 and 1100, respectively. As expected, the studied membranes showed a strong hydrophilic characteristic, in view of the low values of contact angles found. The images also show the high tendency of the liquid to spread over the membrane surface, since the shape of the liquid drop is almost imperceptible due to its rapid absorption.

Figure 11 shows the water flux measured after 60 min of test as a function of sintering temperature and different transmembrane pressures. The permeated water flux is directly influenced by the sintering temperature and transmembrane pressure. A decrease in the water flux was observed with increasing temperature, which is in total agreement with the decrease of porosity. The increasing temperature promotes the filling of pores by the formation of liquid phase, leading a reduction of porosity and consequently reduction of the permeated water flux. Also, the water flux was found to vary linearly with transmembrane pressure. The highest values of water flux were obtained for the membranes sintered at 1025 °C, reaching a value of 302.4 L/hm^2 at 3 bar. However, at a higher sintering temperature of 1100 °C, the water flux of the membrane declined to 142.3 L/hm^2 at 3 bar. From Figure 11, the water permeabilities of the membranes sintered at 1025, 1050, 1075 and 1100 °C are 101.9, 74.7, 73.6 and 45.4 L/hm^{2}bar, respectively. These results were very similar to those reported by Harabi et al.[60], who used a clay composition to obtaining tubular membranes with porosity of 49.0%, average pore size of 0.6 µm, water flux of 300 L/hm^{2}bar at 3 bar and a water permeability of 107 L/hm^{2}bar. Bakhtiari et al.[22] obtained a kaolin tubular membrane with porosity of 33.5%, average pore size of 0.6 µm and water flux of 225 L/hm^2 at 3 bar.

To evaluate the efficiency of theses membranes, an oil water emulsion with a concentration of 200 mg/L was used for separation tests and experiments were conducted at a transmembrane pressure of 3 bar. Figure 12 shows the evolution of permeate flux as function of time of the membranes. It is also observed that the permeate flux for oil in water emulsion is much lower than pure water flux at the same applied pressure. The permeate flux for emulsion shows a pronounced decline in the beginning of operation and stabilizing after 60 min reaching values of 38.8, 23.0, 17.7 and 21.4 L/hm^2 for the membranes sintered at 1025, 1050, 1075 and 1100 °C, respectively. The steady state flux for emulsion is found to be 2.8 – 4.6 times less than the flux at the beginning of filtration. This decline may be related to two significant problems associated to membrane fouling process: concentration polarization and pore blocking[3,5,25,26,61]. At the initial filtration stage, a pore blocking mechanism causes a decrease of permeate flux due the formation of a layer of oil droplets on the membrane surface. Oil droplets move to pores of the membranes and get absorbed on pore walls and membrane surface leading to the filling of pores with increase in filtration time causing a rapid decrease of permeate flux. As the filtration time increased, a cake layer

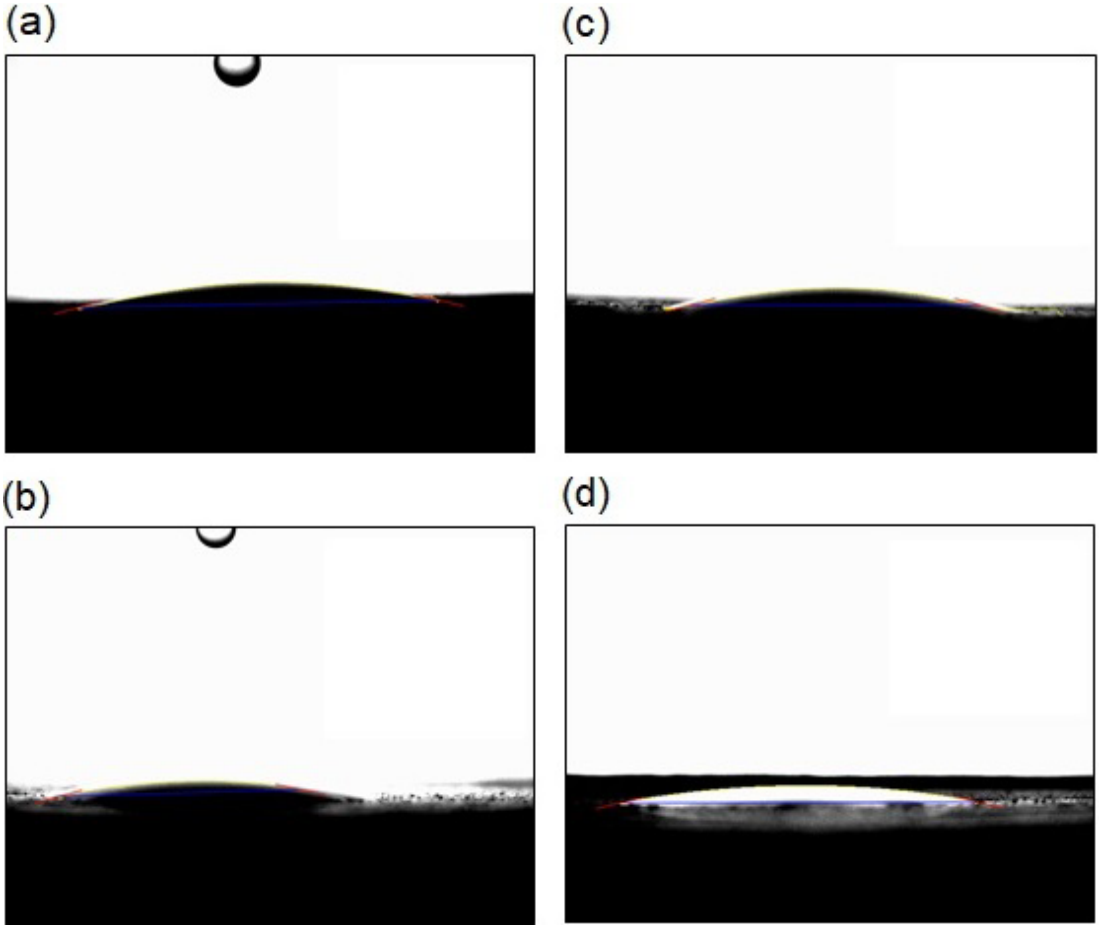

Figure 10. Contact angle measurements of the prepared membranes sintered at (a) 1025, (b) 1050, (c) 1075 and (d) 1100.

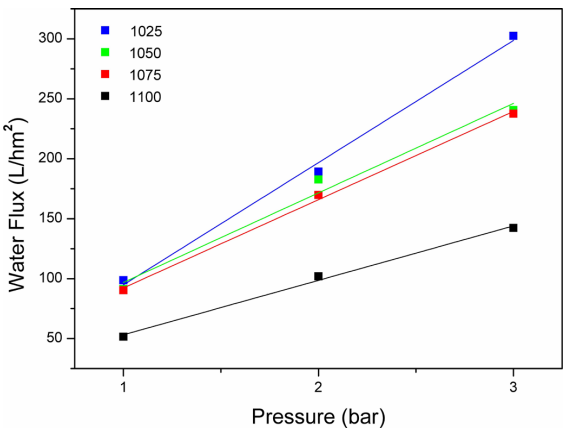

Figure 11. Permeated water flux after 60 min of filtration as a function of transmembrane pressure and different sintering temperature.

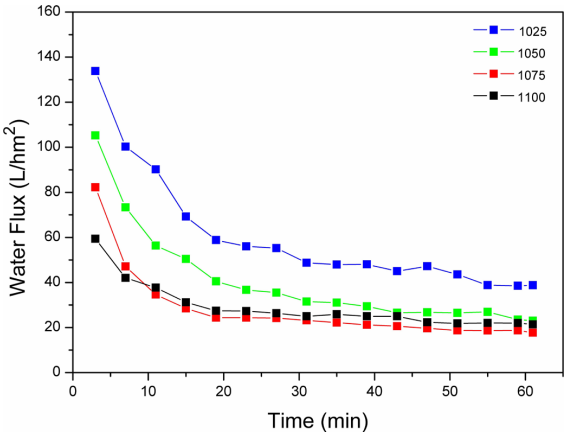

Figure 12. Permeated flux as a function of time of ceramics membranes for oil-water emulsion at a pressure of 3 bar.

forms at the membrane surface and the flux reaches the steady state[3,26]. This cake layer formed act as an additional resistance that prevents the passage of the oil particles through the membrane promoting the increase of oil rejection[24]. However, in the case of tangential flow filtration, if the conditions are correctly selected and the design (chamber diameter) is carried out properly, this effect can be limited. Also, in industrial applications, the flow is recovered by applying back-flash pulse.

Table 2 shows the turbidity results for oil-water emulsion before and after 60 min of permeation tests. As can be seen, the turbidity found for oil-in-water emulsion before pass through the membranes was 65.7 NTU. After 60 minutes of separation tests, the turbidity reduced to 0.06, 0.08, 0.28

Table 2. Turbidity results of oil-in-water emulsion before and after filtration tests.

Sample	Emulsion	1025	1050	1075	1100
Turbidity (NTU)	65.7	0.06	0.08	0.28	0.55
Oil Rejection (%)	-	99.91	99.88	99.57	99.16

Table 3. Details of cost estimation for fabrication of tubular membranes

Cost of raw materials			
Raw materials	Unit price per Kg (R$)	Amount of raw materials (g)	Cost (R$)
Ball Clay	0.38	64.40	0.02
Alumina	3.80	53.20	0.20
Talc	0.45	162.40	0.07
Total raw materials cost for fabrication of forty membranes			0.29
Energy cost (based on the power consumption)			
Mixer			0.36
Dry oven			1.43
Extruder			0.40
Furnace			36.50
Total production cost for fabrication of forty membranes			38.98
Total production cost of one membrane ($1.86x10^{-3}$ m^2) (R$*/US$**)			0.97 (0.18)
Total production cost of membrane (US$/$m^2$)			**97**

*Brazilian currency. **United Sates Dollar (1US$ = R$ 5.45; the price was estimated on 1st February of 2021 by Central Bank of Brazil).

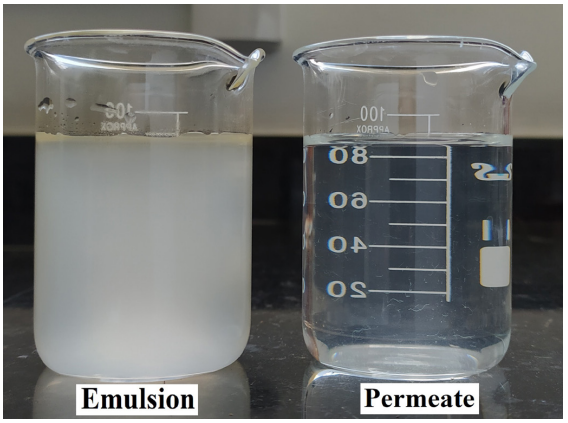

Figure 13. Images of oil-in-water emulsion and permeate.

and 0.77 NTU for the membranes sintered at 1025, 1050, 1075 and 1100 ° C, respectively. According to these results, the membranes promoted high separation efficiency since that the oil rejection was above 99.0% for all membranes as shown in the Table 2. In Figure 13 it is also observed the difference of turbidity between the oil-water emulsion and the permeated, which confirm the high retention of oil particles after filtration tests. From an industrial point of view, the membranes should possess higher removal efficiency with adequate permeability. The prepared membranes in this study showed excellent oil rejection and reasonable permeability when compared to those reported in the literature[26,29,61].

A cost analysis of the prepared membranes is shown in Table 3. The cost was estimated based on the price of raw materials and the energy cost of shaping, drying and sintering process. The production cost is evaluated to be 0.18 US$/membrane or 97 US$/m^2. Comparatively, the membrane cost reported by Bose and Das[62] is 250 US$/$m^2$ and those reported by Ghosh et al.[63] are 172 and 197 US$/$m^2$. Also, the prepared membranes are very much cheaper than commercial ceramic membranes made of α-alumina (US$ 500-1000/m^2) since that the price of alumina is about 100 times that of kaolin and requires sintering temperature above 1600 °C[64]. In our study, the sintering temperature used was lower than 1200 °C, which contribute with economic reduction of energy cost in membrane manufacturing. In conclusion, using raw materials similar to those used in the brick industry, with 20% low-cost alumina, and slightly higher temperatures (1025ºC-1100ºC), the cost is estimated to be 97 US$/$m^2$.

4. Conclusions

In this study, it was emphasized the preparation and application of clay-based membranes oil-water separation. The formulation studied showed an appropriate chemical composition to formation of an important mineralogical phase such as cordierite, which was identified in the samples sintered from 1125 °C and have strongly influenced the mechanical properties of the ceramic membranes. It was also verified that the membranes sintered between 1025 and 1100 °C showed satisfactory porosity and average pore size suitable to be used in separation processes in the microfiltration range. In this way, these membranes were subjected to tangential flow tests with distilled water and oil in water emulsion. The membrane sintered at 1025 °C shows high reasonable permeability and excellent oil rejection. The prepared membranes in this study can be applied in oil-water emulsion separation process. Also, these membranes are considered very inexpensive due the low cost of raw materials and low sintering temperature.

5. Acknowledgements

Authors acknowledge financial support received from CAPES – Brazil (scholarship for Mykaell Y. M. Souza) and CNPq – Brazil (proc. 304643/2015-7 and 308912/2016-0).

6. References

1. Majouli A, Tahiri S, Alami Younssi S, Loukili H, Albizane A. Elaboration of new tubular ceramic membrane from local Moroccan Perlite for microfiltration process: application to treatment of industrial wastewaters. Ceram Int. 2012;38(5):4295-303.
2. Nandi BK, Moparthi A, Uppaluri R, Purkait MK. Treatment of oily wastewater using low cost ceramic membrane: comparative assessment of pore blocking and artificial neural network models. Chem Eng Res Des. 2010;88(7):881-92.
3. Chen M, Zhu L, Dong Y, Li L, Liu J. Waste-to-resource strategy to fabricate highly porous whisker- structured mullite ceramic membrane for simulated oil-in-water emulsion wastewater treatment. ACS Sustain Chem& Eng. 2016;4(4):2098-106.
4. Nath K, editor. Membrane separation process. New Delhi: Pretice-Hall of India; 2017.
5. Belibi Belibi P, Nguemtchouin MMG, Rivallin M, Ndi Nsami J, Sieliechi J, Cerneaux S, et al. Microfiltration ceramic membranes from local Cameroonian clay applicable to water treatment. Ceram Int. 2015;41(2):2752-9.
6. Ben Ali M, Hamdi N, Rodriguez MA, Srasra E. Macroporous ceramic supports from natural clays. Improvement by the use of activated clays. Ceram Int. 2017;43(1):1248.
7. Das B, Chakrabarty B, Barkakati P. Preparation and characterization of novel ceramic membranes for micro-filtration application. Ceram Int. 2016;42(13):14326-33.
8. Achiou B, Elomari H, Bouazizi A, Karim A, Ouammou M, Albizane A, et al. Manufacturing of tubular ceramic microfiltration membrane based on natural pozzolan for pretreatment of seawater desalination. Desalination. 2017;419:181-7.
9. Hedfi I, Hamdi N, Rodriguez MA, Srasra E. Development of a low cost micro-porous ceramic membrane from kaolin and alumina, using the lignite as porogen agent. Ceram Int. 2016;42(4):5089-93.
10. Kouras N, Harabi A, Bouzerara F, Foughali L, Policicchio A, Stelitano S, et al. Macro-porous ceramic supports for membranes prepared from quartz sand and calcite mixtures. J Eur Ceram Soc. 2017;37(9):3159-65.
11. Lorente-Ayza MM, Orts MJ, Gozalbo A, Mestre S. Preparation of chamottes as a raw material for low-cost ceramic membranes. Int J Appl Ceram Technol. 2016;13(6):1149-58.
12. Misrar W, Loutou M, Saadi L, Mansori M, Waqif M, Favotto C. Cordierite containing ceramic membranes from smectetic clay using natural organic wastes as pore-forming agents. Journal of Asian Ceramic Societies. 2017;5(2):199-208.
13. Lorente-Ayza MM, Mestre S, Menéndez M, Sánchez E. Comparison of extruded and pressed low cost ceramic supports for microfiltration membranes. J Eur Ceram Soc. 2015;35(13):3681-91.
14. Zhou J, Zhang X, Wang Y, Larbot A, Hu X. Elaboration and characterization of tubular macroporous ceramic support for membranes from kaolin and dolomite. J Porous Mater. 2010;17(1):1-9.
15. Andrade RM, Jaques NG, Sousa J, Dutra RPS, Macedo DA, Campos LFA. Preparation of low-cost ceramic membranes for microfiltration using sugarcane bagasse ash as a pore-forming agent. Ceramica. 2019;65(376):620-5.
16. Silva MC, Lira HL, Lima RCO, Freitas NL. Effect of sintering temperature on membrane manufactured with clays for textile effluent treatment. Adv Mater Sci Eng. 2015;2015:1-7.
17. Silva FA, Lira HL. Preparação e caracterização de membranas cerâmicas de cordierita. Ceramica. 2006;52(324):276-82.
18. Aissat M, Hamouda S, Bettahar N, Tarboush BJA, Bahmani A. Characterization and application of ceramic membranes prepared from Algerian Kaolin. Ceramica. 2019;65(376):554-61.
19. García E, Gancedo JR, Gracia M. Effect of cycled combustion ageing on a cordierite burner plate. Mater Charact. 2010;61(11):1147-56.
20. Vinoth Kumar R, Kumar Ghoshal A, Pugazhenthi G. Elaboration of novel tubular ceramic membrane from inexpensive raw materials by extrusion method and its performance in microfiltration of synthetic oily wastewater treatment. J Membr Sci. 2015;490:92-102.
21. Bissett H, Zah J, Krieg HM. Manufacture and optimization of tubular ceramic membrane supports. Powder Technol. 2008;181(1):57-66.
22. Bakhtiari O, Samei M, Taghikarimi H, Mohammadi T. Preparation and characterization of mullite tubular membranes. Desalination Water Treat. 2011;36(1-3):210-8.
23. Abbasi M, Mirfendereski M, Nikbakht M, Golshenas M, Mohammadi T. Performance study of mullite and mullite-alumina ceramic MF membranes for oily wastewaters treatment. Desalination. 2010;259(1-3):169-78.
24. Garmsiri E, Rasouli Y, Abbasi M, Izadpanah AA. Chemical cleaning of mullite ceramic microfiltration membranes which are fouled during oily wastewater treatment. J Water Process Eng. 2017;19:81-95.
25. Vasanth D, Pugazhenthi G, Uppaluri R. Fabrication and properties of low cost ceramic microfiltration membranes for separation of oil and bacteria from its solution. J Membr Sci. 2011;379(1-2):154-63.
26. Abbasi M, Mowla D. Analysis of membrane pore-blocking models applied to the MF of real oily wastewaters treatment using mullite and mullite-alumina ceramic membranes. Desalination Water Treat. 2014;52(13-15):2481-93.
27. Eom J-H, Yeom H-J, Kim Y-W, Song I-H. Ceramic membranes prepared from a silicate and clay-mineral mixture for treatment of oily wastewater. Clays Clay Miner. 2015;63(3):222-34.
28. Brasil. Resolução Conama nº 393, de 8 de agosto de 2007. Dispõe sobre o descarte contínuo de água de processo ou de produção em plataformas marítimas de petróleo e gás natural, e dá outras providências. Diário Oficial da União; Brasília; 9 agosto 2007.
29. Suresh K, Pugazhenthi G. Development of ceramic membranes from low-cost clays for the separation of oil – water emulsion. Desalination Water Treat. 2014;57(5):1927-39.
30. Abbasi M, Salahi A, Mirfendereski M, Mohammadi T, Rekabdar F, Hemmati M. Oily wastewater treatment using mullite ceramic membrane. Desalination Water Treat. 2012;37(1-3):21-30.
31. Kumar RV, Monash P, Pugazhenthi G. Treatment of oil-in-water emulsion using tubular ceramic membrane acquired from locally available low-cost inorganic precursors. Desalination Water Treat. 2016;57(58):28056-70.
32. Jiang F, Li Y, Zhao L, Cang D. Novel ceramics prepared from inferior clay rich in CaO and Fe_2O_3: properties, crystalline phases evolution and densification process. Appl Clay Sci. 2017;143:199-204.
33. Zhao L, Li Y, Zhou Y, Cang D. Preparation of novel ceramics with high CaO content from steel slag. Mater Des. 2014;64:608-13.
34. Souza AE, Teixeira SR, Santos GTA, Longo E. Addition of sedimentary rock to kaolinitic clays: influence on sintering process. Ceramica. 2013;59(349):147-55.
35. Wang S. Effects of Fe on crystallization and properties of a new high infrared radiance glass-ceramics. Environ Sci Technol. 2010;44(12):4816-20.
36. Lao X, Xu X, Jiang W, Liang J, Miao L, Wu Q. Influences of impurities and mineralogical structure of different kaolin minerals on thermal properties of cordierite ceramics for high-temperature thermal storage. Appl Clay Sci. 2020;187:1054-85.
37. Gonçalves WP, Silva VJ, Menezes RR, Neves GA, Lira HL, Santana LNL. Mycrostructural, physical and mechanical behavior of pastes containing clays and alumina waste. Appl Clay Sci. 2017;137:259-65.
38. Santos PDS. Ciência e tecnologia de argilas. São Paulo: Edgard Bluvher; 1989.

39. Dong Y, Liu X, Ma Q, Meng G. Preparation of cordierite-based porous ceramic micro-filtration membranes using waste fly ash as the main raw materials. J Membr Sci. 2006;285(1-2):173-81.
40. Al-Harbi OA, Hamzawy EMA. Nanosized cordierite-sapphirine-spinel glass-ceramics from natural raw materials. Ceram Int. 2014;40(4):5283-8.
41. Barba A, Beltrán V, Feliu C, Garcia J, Ginés F, Sánchez E, et al. Materias primas para la fabricación de soportes de baldosas cerámicas. Castellón de la Plana: Instituto de Tecnología Cerámica; 1997.
42. Bejjaoui R, Benhammou A, Nibou L, Tanouti B, Bonnet JP, Yaacoubi A, et al. Synthesis and characterization of cordierite ceramic from Moroccan stevensite and andalusite. Appl Clay Sci. 2010;49(3):336-40.
43. Khabas TA, Vereshchagin VI, Vakalova TV, Kirchanov AA, Kulikovskaya NA, Kozhevnikova NG. Low-temperature synthesis of the cordierite phase in ceramic mixtures of natural raw materials. Refract Ind Ceram. 2003;44(3):181-5.
44. Hajjou H, Saâdi L, Waqif M. Synthesis of cordierite using industrial waste fly ash. Arab J Geosci. 2017;10(359):1-9.
45. Shu C, Mingxia X, Cailou Z, Jiaqi T. Fabrication of cordierite powder from magnesium-aluminum hydroxide and sodium silicate: its characteristics and sintering. Mater Res Bull. 2002;37(7):1333-40.
46. Majumder M, Mukhopadhyay S, Parkash O, Kumar D. Sintering and crystallisation behaviour of chemically prepared cordierite for application in electronic packaging. Ceram Int. 2004;30(6):1067-70.
47. Al-Harbi OA, Ozgur C, Khan MM. Fabrication and characterization of single phase cordierite honeycomb monolith with porous wall from natural raw materials as catalyst support. Ceram Int. 2015;41(3):3526-32.
48. Miyashiro A, Iiyama T, Miyashiro T, Yamasaki M. The polymorphism of cordierite and indialite. Am J Sci. 1955;253(4):185-208.
49. Li Y, Qian H, Cheng X, Zhang R, Zhang H. Fabrication of dense cordierite ceramic through reducing Al_2O_3 mole ratio. Mater Lett. 2014;116:262-4.
50. Li Y, Cheng X, Zhang R, Wang Y, Zhang H. Effect of excess MgO on the properties of cordierite ceramic sintered by solid-state method. Int J Appl Ceram Technol. 2015;12(2):443-50.
51. Nath SK, Kumar S, Kumar R. Effect of mechanical activation on cordierite synthesis through solid-state sintering method. Bull Mater Sci. 2014;37(6):1121-6.
52. Goren R, Ozgur C, Gocmez H. The preparation of cordierite from talc, fly ash, fused silica and alumina mixtures. Ceram Int. 2006;32(1):53-60.
53. Gökçe H, Aĝaoĝullari D, Öveçoĝlu ML, Duman I, Boyraz T. Characterization of microstructural and thermal properties of steatite/cordierite ceramics prepared by using natural raw materials. J Eur Ceram Soc. 2011;31(14):2741-7.
54. Liu C, Liu L, Tan K, Zhang L, Tang K, Shi X. Fabrication and characterization of porous cordierite ceramics prepared from ferrochromium slag. Ceram Int. 2016;42(1):734-42.
55. Benhammou A, El Hafiane Y, Abourriche A, Abouliatim Y, Nibou L, Yaacoubi A, et al. Effects of oil shale addition and sintering cycle on the microstructure and mechanical properties of porous cordierite-ceramic. Ceram Int. 2014;40(7):8937-44.
56. Fakhfakh S, Baklouti S, Baklouti S, Bouaziz J. Elaboration and characterisation of low cost ceramic support membrane. Adv Appl Ceramics. 2010;109(1):31-8.
57. Saffaj N, Persin M, Younsi SA, Albizane A, Cretin M, Larbot A. Elaboration and characterization of microfiltration and ultrafiltration membranes deposited on raw support prepared from natural Moroccan clay: application to filtration of solution containing dyes and salts. Appl Clay Sci. 2006;31(1-2):110-9.
58. Ghouil B, Harabi A, Bouzerara F, Boudaira B, Guechi A, Demir MM, et al. Development and characterization of tubular composite ceramic membranes using natural alumino-silicates for microfiltration applications. Mater Charact. 2015;103:18-27.
59. Ohji T, Fukushima M. Macro-porous ceramics: processing and properties. Int Mater Rev. 2012;57(2):115-31.
60. Harabi A, Bouzerara F, Condom S. Preparation and characterization of tubular membrane supports using centrifugal casting. Desalination Water Treat. 2009;6(1-3):222-6.
61. Arzani M, Mahdavi HR, Bakhtiari O, Mohammadi T. Preparation of mullite ceramic microfilter membranes using Response surface methodology based on central composite design. Ceram Int. 2016;42(7):8155-64.
62. Bose S, Das C. Preparation and characterization of low cost tubular ceramic support membranes using sawdust as a pore-former. Mater Lett. 2013;110:152-5.
63. Ghosh D, Sinha MK, Purkait MK. A comparative analysis of low-cost ceramic membrane preparation for effective fluoride removal using hybrid technique. Desalination. 2013;327:2-13.
64. Kaur H, Bulasara VK, Gupta RK. Effect of carbonates composition on the permeation characteristics of low-cost ceramic membrane supports. J Ind Eng Chem. 2016;44:185-94.